Lossy Mode Resonance Based 1-Butanol Sensor in the Mid-Infrared Region

E.E. Gallego Martínez[a, b*], I.R. Matías[a, c], S. Melendi-Espina[d], M. Hernáez[d], C. Ruiz Zamarreño[a, c]

[a] *Electrical, Electronic and Communications Engineering Department in the Public University of Navarra, Pamplona, 310016 Spain*

[b] *Telecommunications and Electronic Department at the University of Pinar del Río, Pinar del Río, 20100, Cuba*

[c] *Institute of Smart Cities, Jeronimo de Ayanz Building, Pamplona, 310016 Spain*

[d] *School of Engineering, University of East Anglia (UEA), Norwich Research Park, Norwich NR4 7TJ, UK*

ARTICLE INFO

Lossy Mode Resonance

Infrared Optical Gas Sensor

1-Butanol sensor

Fluorinated Materials

Graphene Oxide

ABSTRACT

The utilization of nanometric Graphene Oxide / Polyethyleneimine (GO/PEI) bilayers deposited onto SnO_2-coated CaF_2 planar waveguides significantly enhances the sensitivity of Lossy Mode Resonances (LMR) based devices for gas sensing applications. LMR generation in the mid-infrared region, which also contributed to achieve better sensitivities, was accomplished with the aid of fluorinated (CaF_2) planar waveguides. LMR wavelength shift was studied as a function of the number of GO/PEI bilayers. In the particular case of 10 bilayers of GO/PEI, the sensitivity of the device to 1-butanol was 70.4 pm/ppm, which increased by a factor of 5 compared to the device without GO/PEI bilayers. The GO/PEI sensor was also sensitive to other alcohols, like 2-propanol, but it showed negligible sensitivity to other gases, such as CO_2, NH_3 or C_2H_2. The cross sensitivity with temperature was tested at temperatures of 20, 100 and 180 ºC during water vapor measurement (1723 ppm), showing that the sensor performance was not affected by the temperature fluctuations.

* Corresponding author:
Email-address: elieser.gallego@unavarra.es (E.E. Gallego Martínez)

Received XX February 2023; Received in revised form XX February 2023; Accepted XX February 2023
Available online XX February 2023

1. Introduction

Lossy mode resonances (LMR) may occur when a thin film is deposited on a waveguide fulfilling some conditions. Specifically, if the optical characteristics of the thin-film material match the conditions for LMR generation, some of the modes will shift from being transmitted through the waveguide to being transmitted through the thin film [1]. Basically, the necessary conditions for the LMR to occur are: the real part of the permittivity in the thin film has to be greater than cero and its module greater than both, the module of its imaginary part and the module of the imaginary part of the material surrounding the film [2, 3]. The result is the generation of an attenuation band in the spectrum of the optical signal transmitted through the system, known as LMR. LMRs can be obtained with both transverse electric (TE) and transverse ~~electric~~ magnetic (TM) polarizations, and it is possible to generate multiple attenuation bands in the transmitted spectrum depending on the thickness of the thin film and the refractive index (RI) of the materials. It is possible to describe the behavior of external parameters monitoring the central wavelength of the optical resonance [1].

LMRs have been successfully obtained using optical fiber waveguides and thin films of several metal oxides, such as indium tin oxide (ITO) [1], indium oxide [4], tungsten oxide [5], tin oxide [6], zinc oxide [7], aluminum-doped zinc oxide [8], copper oxide [9] and iron oxide nanostructures combined with tin oxide [10]; also, polymeric coatings [11] have been used to generate LMR. Recently, planar waveguides combined with thin film materials have been successfully proposed as an alternative candidate for the fabrication of LMR based devices [12, 13]. Planar waveguide approach is less brittle than optical fiber, facilitates the thin film fabrication processes generally intended for planar surfaces and enables a greater variety in the number of materials available compared with that of optical fiber.

LMR effect in fiber optics has demonstrated to be successful for the detection of ammonia [14], humidity [15, 16, 17, 18, 19, 20, 21, 22, 23], ethanol [24] and hydrogen sulfide [25]. Recently, planar waveguides have also been proven successfully for acetone, water vapor and ethanol detection [26]. In this latter work, the

material used to generate the LMR was graphene oxide (GO*)* deposited onto cover slides utilized as waveguide [26].

Some of the above-mentioned studies [7, 10, 19, 22] use nanostructures, such as nanorods, to maximize the surface area in direct contact with the gas target and, therefore, improve the sensor's performance. In other works, a sensitive coating containing relevant functional groups is used for the detection of some specific gaseous compounds, as it was the case of GO [24, 26].

GO, a non-stoichiometric compound and precursor of graphene materials, contains various types of oxygen moieties, including epoxy, hydroxyl, carboxylic and carbonyl groups. The hydroxyl and epoxide functional groups are located on its basal plane, and carbonyl and carboxyl functionalities on its edges (according to the variations of the Lerf-Klinowski model [27, 28], the most accepted model in the scientific literature). GO has demonstrated its suitability in combination with the LMR effect to design optical sensors (fiber optics and planar waveguides) for the detection of ethanol, acetone, humidity, and ammonia, amongst others [24, 25]. However, it is worth mentioning that all these studies have been focused on the visible region of the spectrum, where the sensitivity is lower than that of the mid infrared region (MIR). Moreover, many strong absorption lines can be found in the MIR wavelength region associated to rotational and vibrational changes of molecules [29], which shows significant potential for a new generation of devices in this region targeting applications for breath analysis in medical applications or exhaust gases in industrial sectors [30].

Butanol (butyl alcohol) is an aliphatic saturated C_4 alcohol (C_4H_9OH, 74.12 g/mole) with four structural isomers: *n*-butanol, isobutanol, *sec*-butanol and *tert*-butanol. Due to an asymmetric C atom in the secondary alcohol, there are two stereoisomers of 2-butanol. 1-butanol is a natural product found in some organisms in nature, however it is primarily obtained by fermentation [31]. 1-butanol has been presented as an exhaled air biomarker for lung cancer [32]. 1-butanol is the gas that presents the highest concentration in the exhaled breath of patients with lung cancer in all the stages of the disease. As a consequence, 1-butanol can be used as lung cancer biomarker. Therefore, the development of simple and accurate 1-butanol detection tools in exhaled breath have excellent potential for applications in lung cancer detection and diagnosis [32].

Furthermore, World Health Organization (WHO) has fixed 20 ppm of 1-butanol as the threshold risk level for professional and work environment [33], according to the risk level to human health. Moreover, other studies have reported that concentrations in air exceeding 50 ppm can produce ocular irritation, disgusting odor, slight headache and dizziness, nose and throat irritation and dermatitis in fingers and hands [34]. Thus, 1-butanol detection is of great importance in terms of safety and healthcare.

So far, different approaches for 1-butanol detection have been explored using a variety of materials and technologies comprising but not limited to the following:

- AuNPs-modified $Fe_2O_3/ZnFe_2O_4$ heterostructures, which can detect 1-butanol concentrations in the ppb range, while operating at temperatures from 100 ºC to 340 ºC [35].
- ZnOMWCNT nanocomposites, which take advantage of the chemisorption electron conduction phenomena. These devices accomplish 1-butanol detection limits from 50 ppm to 500 ppm at room temperature [36].
- QCM coated with co-polymer P(HEMA-co-MA), achieving 1-butanol detection down to 72 ppm also at room temperature [37].
- The integration of a thin film of ZnO and an inter-digitated electrode fabricated on a flexible Teflon substrate for tested sensitivity between 50 ppm and 100 ppm at 27 ºC [38].
- In the field of optical sensors, an “optical nose” based on Au@MOFs nanoparticles arrays through surface/enhanced Raman scattering [39] achieved to detect a 1-butanol concentration of 1000 ppm.

Table 1 shows a summary of the mentioned of 1-butanol sensors found in the literature.

Table 1: Summary of 1-Butanol sensors performance.

Sensor technology	Detection limit [ppm]	Operating temperature [ºC]	Response / Recovery times [s]	Reference
Electro-chemical	0.05	100 – 340	6 / 16	[35]
Electro-chemical	50	Room temperature	60 / 80	[36]
Electro-chemical	72	Room temperature	Not informed	[37]
Electro-chemical	50	27 ºC	62 / 70	[38]
Optical	1000	Room temperature	Not informed	[39]

To avoid ignition risk, it is preferable to operate these sensors at low temperatures. Nevertheless, it is still challenging to reach 1-butanol detection limits below 50 ppm at room temperature. Consequently, the aim of this work consists of the design and characterization of a highly sensitive GO-based LMR-planar device for 1-butanol gas detection operating at room temperature for its use in different applications in industry and healthcare.

The paper is organized as follows. First, the procedure for the assembly and characterization of the devices is described. Then, studied the sensor fabrication process as a function of the number of GO/PEI bilayers fabricated is studied. Finally, the sensitivity of the obtained devices to 1-butanol is tested together with the cross sensitivity to other gaseous species and temperature.

2. Materials and Methods

2.1. Sensor fabrication

The sensing coating was fabricated by means of Layer-by-Layer (LbL) deposition of GO/PEI bilayers onto a planar CaF_2 substrate, which was priorly coated with a thin film of sputtered SnO_2 (see zoom in Figure 1).

This sputtered layer acted as LMR generator. The thickness of the SnO_2 was controlled to operate at wavelengths close to or greater than 2µm. Having the resonance in the MIR region responds to the direct proportionality relationship between the LMR sensitivity and the square of the wavelength where it occurs [13, 40] according to equation (1). The transmission of light in the MIR region of the spectrum was possible due to the use of fluorinated materials, such as CaF_2, as substrate and ZrF_4 as fiber patch cords (Figure 1).

$$S = \frac{\lambda^2}{2\pi d_2} \frac{\left(\frac{n_2^2}{n_3\sqrt{n_1^2 - n_3^2}} + \frac{2n_2^2\sqrt{n_1^2 - n_3^2}}{n_3^2}\right) n_3^4}{n_2^4(n_2^2 - n_1^2) + n_3^4(n_2^2 - n_1^2)} \qquad (1)$$

Fluorinated Calcium (CaF_2) glass cover slides 10 x 10 x 0.5 mm purchased from UQG Optics were used as substrates. The transmittance of CaF_2 is 90 % up to a wavelength equal to 7 µm when the substrate size is 10 mm, and its refractive index is 1.42 at 2.3 µm [41].

SnO_2 thin films were fabricated onto the CaF_2 substrates by means of DC-sputtering using a Benchtop High-Vacuum Magnetron Sputtering System purchased from MOORFIELD. The substrate was placed into the sputtering chamber, 10 cm under the SnO_2 target. Deposition conditions were 1.2 x 10^{-2} mBar vacuum pressure, 120 mA *DC* current, 20 ºC coolant temperature and 90 min deposition time with rotational speed of 2 s^{-1}. GO/PEI bilayers were deposited onto the SnO_2 covered substrates by means of LbL electrostatic self-assembly, following the procedure explained elsewhere [24].

Before the LbL deposition process, the substrates were cleaned with deionized (DI) water and soap and subsequently submerged into a 1 M KOH solution for 30 minutes. Afterwards, they were cleaned with DI water and dried in air. This process was performed to promote a negative charge in the substrate surface. For the LbL fabrication process, a 0.5 mg/mL GO (from Graphenea, S.A., San Sebastian, Spain) dispersion and 2 mg/mL PEI (from Sigma-Aldrich) solution were employed. Both samples were prepared in DI water. PEI solution was stirred overnight and the GO dispersion was sonicated for two hours prior to deposition to prevent aggregation [24]. The LbL deposition started with the immersion of the substrate into the PEI solution for 5 minutes. Then, it was rinsed in DI water for 1 minute to remove the excess of material and dried in air for 1 min. Afterwards, the substrate was immersed into the GO dispersion for 5 minutes followed by the rinse

and drying processes described before, obtaining the first bilayer of GO/PEI. At the end of each bilayer, the substrate was kept for 5 minutes in an oven at 180 ºC to achieve a stable position of the resonance at the studied spectrum region.

2.2. Experimental setup

The optical experimental set-up used to perform the gas measurements is shown in Figure 1. The setup consisted of a stabilized light source (Thorlabs SLS 201L) that coupled light into the edge of the substrate by means of a ZrF_4 optical fiber (Thorlabs MZ41L1, with a working range up to 4.5 µm). The Arcoptix FTNIR spectrometer (Arcoptix Switzerland, with maximum wavelength range of 2.6 µm) collected the light at the output edge of the substrate using another ZrF4 optical fiber (Thorlabs MZ41L) with a resolution of 4.8 nm at the wavelength of interest (2.2µm). It is worth mentioning that the estimation of the resonance wavelength is not performed directly on the values measured by the spectrometer. However, the parabola method is used to obtain the LMR central wavelength, which allows precise monitoring of the performance of the sensor. As it was previously mentioned, the substrate material, CaF_2, has a transmittance of 90% up to 7 µm. Thus, the working wavelength range in this case was imposed by the spectrometer, which permitted to observe resonances in the range from 0.9 µm to 2.6 µm.

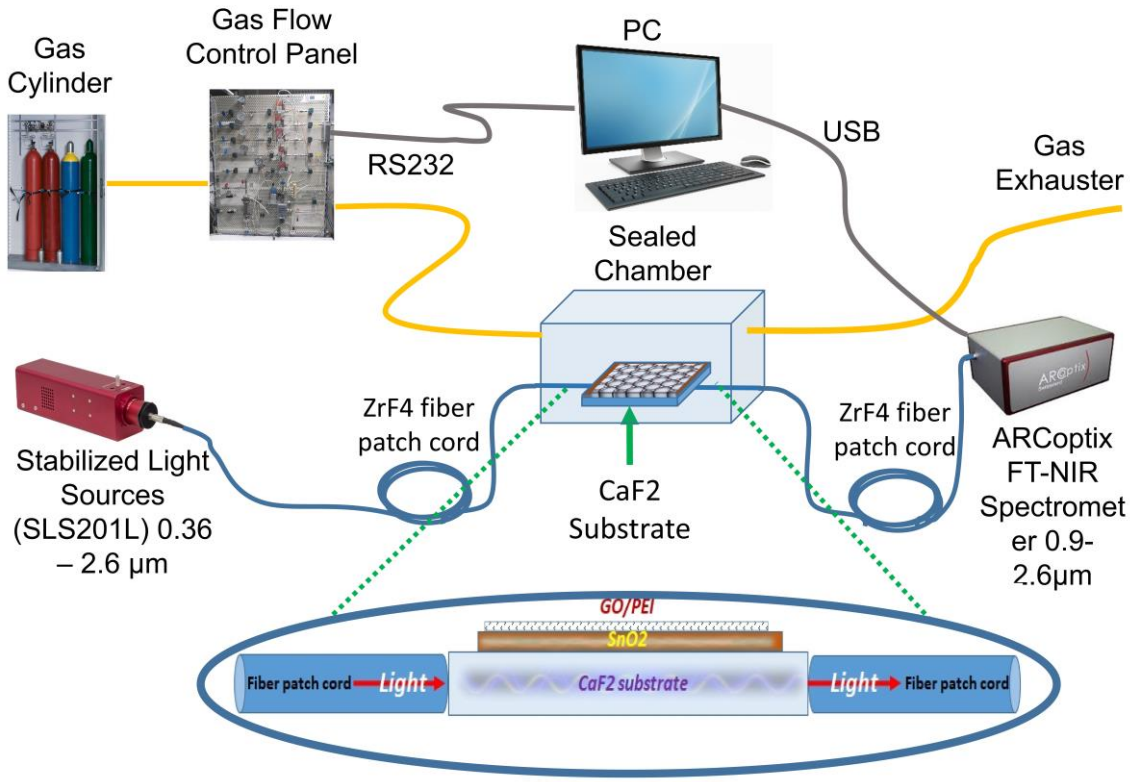

Figure 1: Experimental set-up and sensor structure.

2.3. Gas concentration measurements

Gas measurements were done using a gas flow controller (from Bronkhorst, NL-7261 AK Ruurlo, Netherlands) that permitted to maintain a continuous flow. N_2 gas was used as carrier and mixed with 1-butanol and water vapor using a controlled evaporation mixer (CEM - from Bronkhorst, NL-7261 AK Ruurlo, Netherlands). Since the 1-butanol mass flow was given in mg/h and the nitrogen gas flow in mL/min, it was required a transformation to express the concentration in ppm [42]. Unit transformation was done considering the molar mass of 1-butanol (74,121 g/mole) and the molar volume of gases (22.4 L/mole) in the formula shown in equation (2):

$$Bppm = \frac{Fb}{Fb + Fn} * 10^6 \qquad (2)$$

Where *Fb* is the molar flow of 1-butanol, *Fn* is the molar flow of nitrogen and *Bppm* is the resulting concentration of 1-butanol expressed in ppm.

According to equation (2), the concentration of 1-butanol is shown as a function of the mass flow in Figure 2. N_2 gas flow used during the measurements was kept constant at 300 mL/min to preserve the measuring conditions and the 1-butanol mass flow was kept in the range of 20 to 100 mg/h. A mass flow lower limit of 20 mg/h represented in Figure 2 is associated to the minimum stable concentration permitted by the mass flow controller. Previous limitations permitted to achieve concentrations of 1-butanol in the range of 335 to 1676 ppm. The sensitivity of the obtained devices is determined by the quotient of the LMR wavelength shift (nm) and the gas concentration (ppm).

In the same manner, Figure 2 also shows the concentrations of water vapor and 2-propanol gas, at different mass flow rates for a given N_2 flow of 300 mL/min. The studied concentration range for water vapor and 2-propanol were 3442 - 13627 ppm and 620 - 3713 ppm respectively.

All the measurements were performed at a fixed temperature of 20 ºC, controlled by the *CEM*, except the one described in section *3.3 Temperature cross-sensitivity*. Temperature cross sensitivity study was performed at a constant water vapor concentration of 1723 ppm for three different temperatures (20, 100 and 180 ºC).

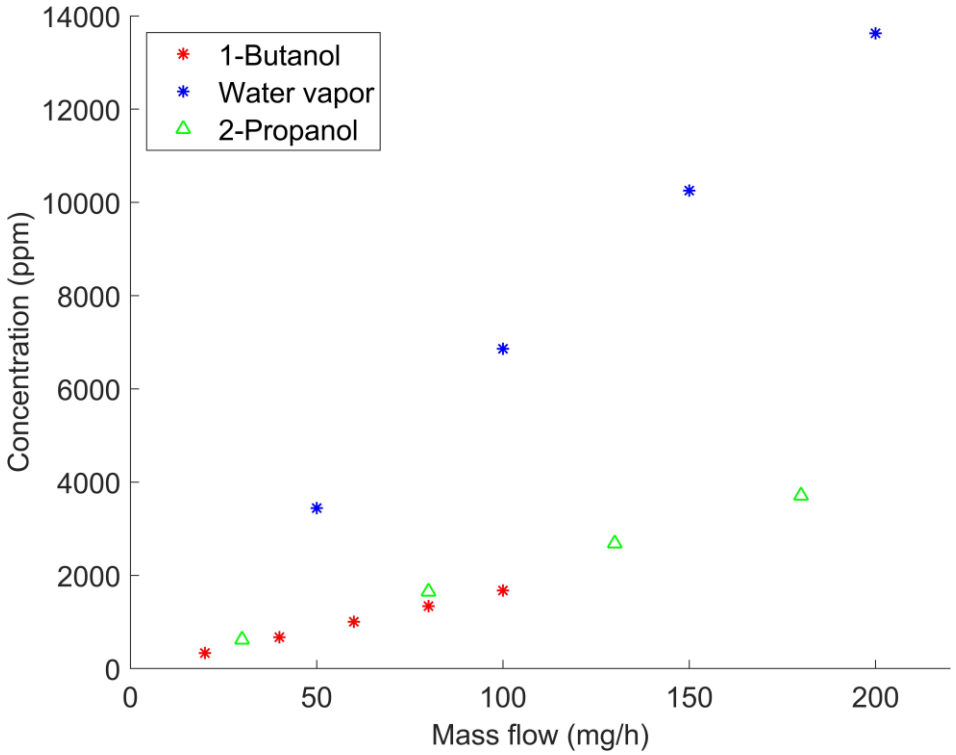

Figure 2: ppm concentrations of 1-butanol, water vapor and 2-propanol in the sealed chamber as function of the mass flow for 300 mL/min N_2 flow.

The response and recovery times are referred to the time required for a sensor to reach 90% and 10% respectively of the final response from a stable condition. All the measurements for the different gaseous species were taken for the lowest concentration measured in that experiment.

The CEM response and recovery times for water vapor and other pressurized liquids were 180 and 93 seconds, respectively. In the case of gas controller, the response and recovery times were 3 and 1 seconds, respectively.

The cross sensitivity of sensor A (with GO/PEI bilayers) was also tested with other gases at different concentrations, such as NH_3 (1890 ppm), C_2H_2 (400 ppm) and CO_2 (10^6 ppm, pure).

Subsequently, the fabricated device was characterized. Cross sensitivity tests at different temperatures were performed, as well as the response of the sensor towards 1-butanol, water vapor and 2-propanol. The impact of the number of bilayers of the GO/PEI coating on the resonance sensitivity was also studied and, accordingly, the suitability of GO for 1-butanol detection demonstrated.

3. Results and Discussion

3.1 Fabrication of the GO/PEI sensitive coating

GO/PEI nanostructured coatings have been presented in previous works as suitable materials for the generation of LMRs [24, 26]. Figure 3 shows the absorption spectrum as a function of the GO/PEI bilayers fabricated onto the CaF_2 substrate. As it can be noted, this approach is not feasible in this case. A direct deposition of GO/PEI bilayers onto the surface of the CaF_2 substrates reveals an increase in absorption in the entire band of the spectrum and no LMR is observed in that region. Therefore, an intermediate LMR generating thin-film, SnO_2, was used prior to the fabrication of the GO/PEI bilayer structure.

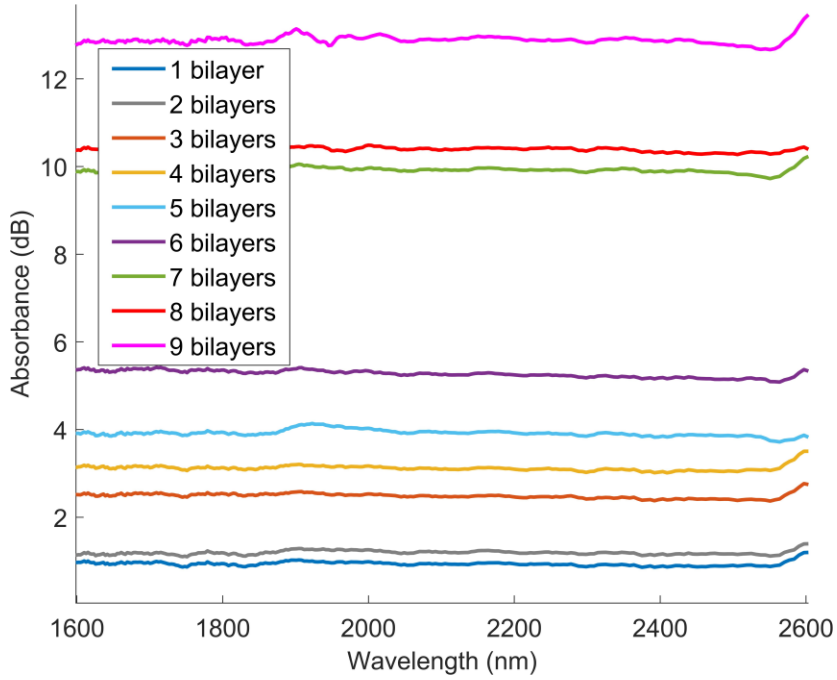

Figure 3: Absorbance spectrum as a function of the GO/PEI bilayers fabricated onto the CaF_2 substrate.

Thus, GO/PEI bilayers were fabricated onto a sputtered SnO_2 thin film, which acted as LMR generator [6]. This resonance was generated at a wavelength of 1976 nm with a thin film of 280 nm.

GO/PEI bilayers are expected to provide the device a gas sensitivity enhancement due to the oxygen functional groups in the chemical structure of the GO at the outer surface [43].

The study of the fabrication of the GO/PEI coatings onto the SnO_2 layer as a function of the number of bilayers is shown in Figure 4. It is observed that the LMR central wavelength changes notably in bilayers 1, 2 and 3 and very slightly from 4-9, vanishing completely in 11, which establishes a limit of 10 bilayers for the utilization of this LMR-based device for sensing purposes. Additionally, the resonance retains the sensitivity to the RI changes despite the increase in the number of GO/PEI bilayers. These shifts were tested from air (RI=1) to water (RI=1.333). For all bilayers it was 318 nm/RIU. Therefore, the final decision was made to carry out the investigation with a structure of 10 bilayers of GO/PEI because it represents a balance between the figure of merit of the LMR resonance and the highest possible number of bilayers, while the amount of GO in the coating, and thus oxygen functional groups, is also maximized. It means that the resonance will be still visible at the absorbance spectrum while the GO sensitive coating will be as sensitive as possible.

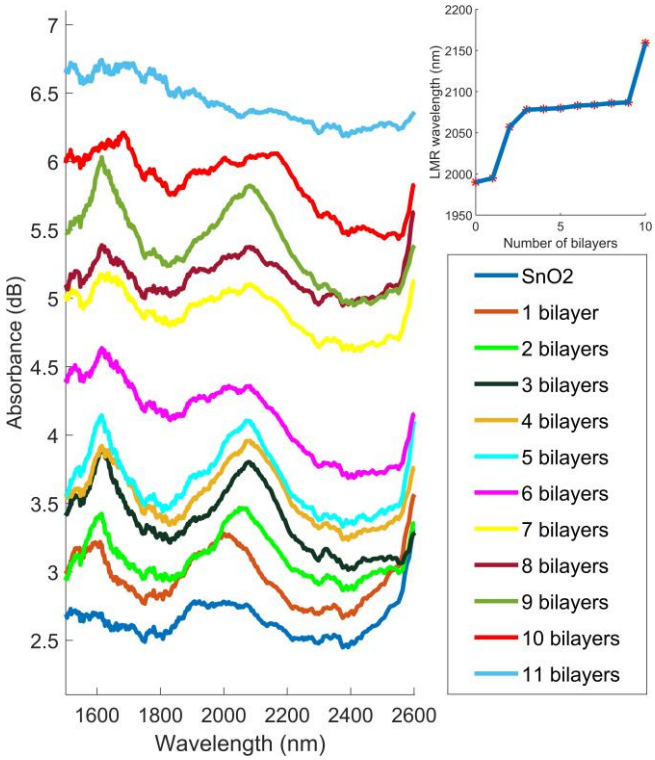

Figure 4: Resonance evolution as function of the number of *GO/PEI* bilayers.

3.2 Gas measurements

In order to study and compare the performance of the devices for gas sensing purposes, a GO/PEI device with 10 bilayers (Sensor A) and the device without the GO/PEI multilayer structure, only with the SnO_2 thin film (Sensor B), were subjected to different concentrations of water vapor and 1-butanol. In the case of water vapor measurement, sensor A shows a sensitivity 5.5 times higher than sensor B (see Figure 5). Specifically, sensitivity of sensor B is 2 pm/ppm and that of sensor A is 11 pm/ppm. The small fluctuations observed for both devices are related to inaccuracies of the CEM. The sensitivity enhancement is mainly associated to the high potential of GO to adsorb and store water molecules owing to the oxygen-containing functional groups on its hydrophilic surface [44].

The response and recovery times of sensor A were 27 and 42 seconds respectively (measured for the lowest concentration). This recovery time is associated to strong interaction between the GO and the water molecules demonstrated in [44], which in turn is due to the exponential dependence of the number of O-H bonds in hydrated GO to the water content [45].

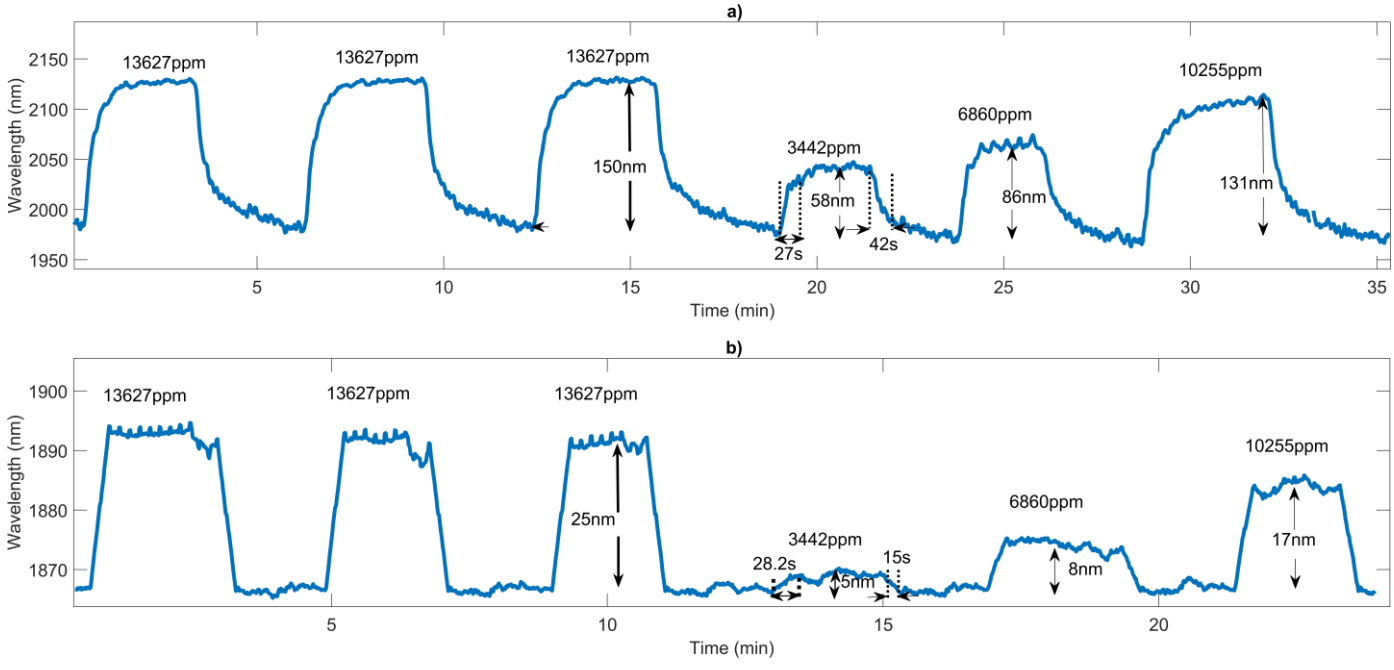

Figure 5: LMR wavelength shift as a function of water vapor concentrations: a) sensor A (with 10 bilayers of *GO/PEI*) and b) sensor B (without *GO/PEI*).

In a same way, Figure 6 shows the response of both, sensor A and sensor B to 1-butanol gas. Sensor A shows a sensitivity of 70.4 pm/ppm, which denotes 5.13 times enhancement compared to sensor B for changes of 1-butanol concentrations in the range from 0 to 1676 ppm. In this interval, sensor B has a sensitivity of 13.7 pm/ppm.

Response and recovery times of sensor A to 1-butanol were 108 and 234 seconds respectively (measured for the lowest concentration).

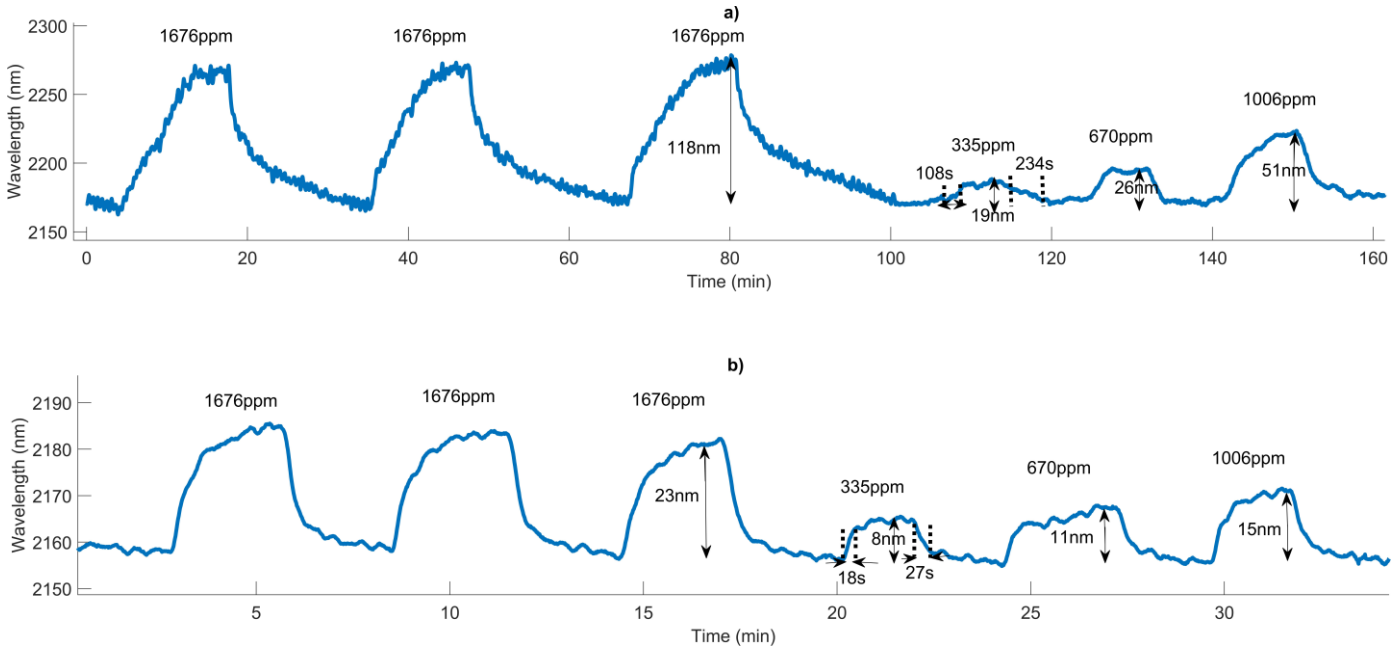

Figure 6: LMR wavelength shift as a function of 1-butanol concentrations: a) sensor A and b) sensor B.

Sensor A exhibits an excellent sensitivity to water vapor and 1-butanol detection in comparison to sensor B. Additionally, the response of sensor A was tested to 2-propanol, a gaseous compound of the same family of 1-butanol. The test was performed at the concentrations indicated in Figure 2 (from 620 ppm to 3723 ppm), and results are shown in Figure 7. Response and recovery times for 2-propanol were 36 and 102 seconds respectively (measured at the lowest concentration).

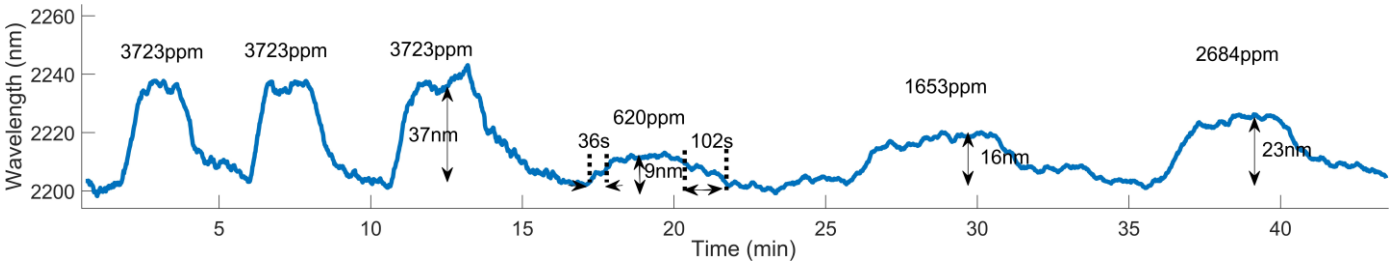

Figure 7: LMR wavelength shift of sensor A as a function of 2-propanol concentrations.

Additional experiments were performed with sensor A to test the cross sensitivity with other gases (NH_3, C_2H_2, and CO_2), showing negligible sensitivity (less than 1%) to NH_3(1890 ppm), C_2H_2 (400 ppm) and CO_2 (10^6 ppm, pure).

Sensor A shown good repeatability in the response to water vapor, 1-butanol and 2-propanol. Figure 8 shows the LMR wavelength shift of sensor A as a function of the measured concentrations of the target gases and includes the standard deviations of the measurements associated to *CEM* inaccuracies.

In the case of water vapor, the LMR wavelength shift shows a linearity factor of R^2=0.970 with the increase of the gas concentration in the measured range, achieving a sensitivity of 11 pm/ppm. Gas sensitivity achieved for 2-propanol was 10 pm/ppm with a linearity factor R^2=0.965. Gas sensitivity for 1-butanol was 70.4 pm/ppm, with a linearity factor R^2=0.876, which reveals the non-linear response of the device to 1-butanol gas, particularly at higher concentrations, which also occurs with other LMR-based optical sensors [6, 46]. This behavior is directly associated with the non-linear adsorption capacity of GO at the external surface of the sensor for higher concentrations of 1-butanol. This was demonstrated in [44] with the exponential adsorption capacity of GO, which depends on the number of O-H bonds that exponentially increases with gas concentrations.

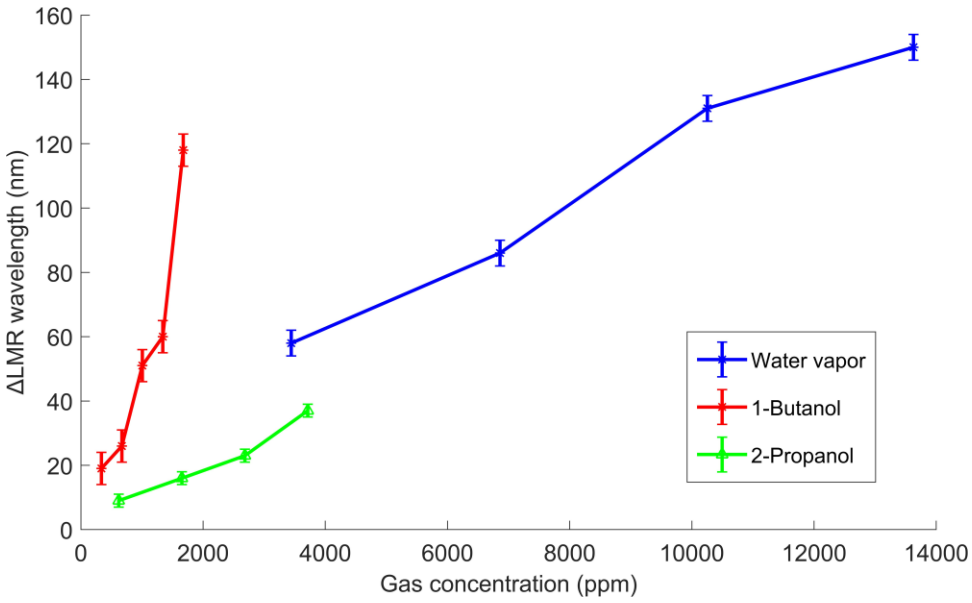

Figure 8: LMR Wavelength shift of sensor A for different concentrations of water vapor, 1-butanol and 2-propanol.

Figure 9 shows a nonlinear adjustment of the behavior of sensor A for the studied concentrations of 1-butanol, by means of a polynomial fit defined by equation (2). The error bars represent the standard deviation produced by the *CEM* inaccuracies. The new R^2 for this polynomial fit is equal to 0.959.

$$p = 5.47 * 10^{-5} x^2 - 0.04081x + 28.22 \qquad (2)$$

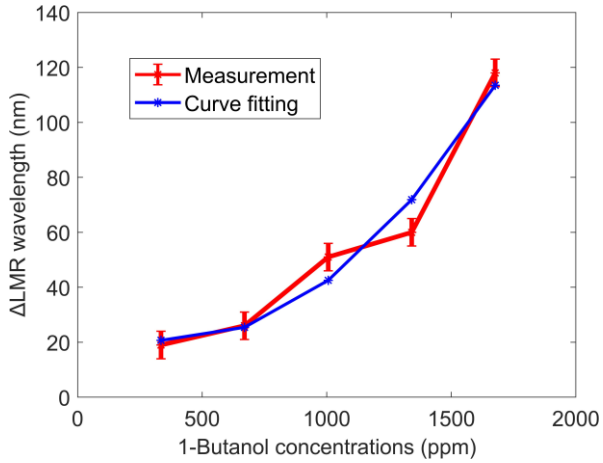

Figure 9: Nonlinear adjustment of sensor A response to 1-butanol.

Table 2 shows a performance index data of sensors A and B.

Table 2: Comparison of performance parameters of sensors A and B.

Sensor	Response time (s)		Recovery time (s)		Sensitivity (pm/ppm)	
	Water vapor	1-butanol	Water vapor	1-butanol	Water vapor	1-butanol
A	27	108	42	234	11	70.4
B	28	18	15	27	2	13.7

Larger response times can be observed for the highest concentrations of 1-butanol. This is associated with two fundamental causes. First, in general it is due to the local stress or strain that must be exerted by the nitrogen flow to expel the 1-butanol out of the sealed chamber system, which is explained by the dynamic viscosity of 1-butanol (2.947 mPa·s at 20 ºC [47]), that is 2.6 times greater than that of the water (1.002 mPa·s at 20 ºC [48]). Second, in the particular case of sensor A, it is due to the exponential dependence of O-H bonds in the hydrated GO structure [45]. Thus, the increase in hydrogen bonding leads to a greater delay in the recovery of the initial resonance wavelength when the 1-butanol is expelled out of the sealed chamber.

However, the only 1-butanol optical sensor found in literature [39] does not offer information about the response and recovery times of 1-butanol detection for comparative purposes. On the other hand, electrochemical sensors require for a concentration of 100 ppm of 1-butanol gas between 6 and 9 seconds of response and recovery time respectively at 200 ºC [35]. These are significantly different operating conditions to those of sensor A, as it was tested at room conditions (20 ºC) and it is not directly comparable.

3.3 Temperature cross-sensitivity

Cross-sensitivity to temperature fluctuations was also tested with sensor A subjected to temperature variations under the same cycles of humidity conditions. Here, the *CEM* was set to heat up to 20 ºC, 100 ºC and 180 ºC for the first, second and third water vapor injection cycles respectively. This test was performed using N_2 as gas carrier with a flow of 300 mL/h. Both temperature transitions took 55±2 sec to complete. Results (see Figure 10) reveal no LMR shift associated to temperature variations, demonstrating that the device provides robust water vapor measurements independent to temperature fluctuations in the range 20

ºC-180 ºC. Temperature tests could not be performed with 1-butanol to prevent CEM damage, since its ignition temperature is 29 ºC. However, it is likely that the device also presents consistent measurements for this alcohol under slight temperature fluctuations.

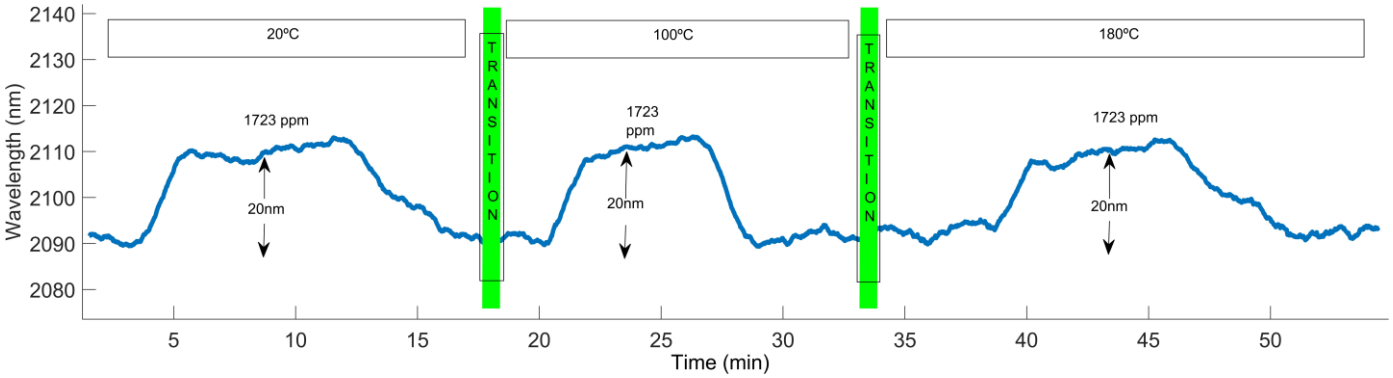

Figure 10: Sensor A: test of temperature sensitivity during the measurement of water vapor for 20, 100 and 180ºC.

4. Conclusions

GO/PEI nanostructured coatings were fabricated directly on the CaF_2 substrate and over a CaF_2 substrate covered with a SnO_2 layer in order to enhance the sensitivity of LMR-based sensors for gas detection. To the best of authors knowledge, in this work LMRs in the MIR region was obtained for the first time using CaF_2 planar waveguides as substrates and sputtered SnO_2 thin films.

Sensitivity enhancement of LMR based gas sensors fabricated on planar waveguides was achieved using GO/PEI bilayers. Sensitivity enhancement for water vapor and 1-butanol gas, achieved a six-fold increase and a fivefold increase respectively. Studied device revealed cross-sensitivity with gaseous compounds of the family of 1-butanol, such as 2-propanol, but negligible response to other gaseous compounds, such as NH_3, C_2H_2 and CO_2. Temperature cross sensitivity studies also exhibited that temperature fluctuations in the range between 20-180 ºC do not affect the performance of the sensor. Consequently, this study reveals the possibility of fabricating robust LMR-based gas sensors on planar waveguides for a variety of applications.

According to the sensitivity to 1-butanol, the developed device could achieve 15 ppm of 1-butanol detection with an optimized gas configuration setup, which make it faceable for environmental monitoring applications.

Credit Authorship Contribution Statement

The contributions of EEGM to the present results were the preparation of the materials, the fabrication of the sensors and the performance of the measurement experiments. MH and SME developed the deposition protocol. CRZ and IRM conceived the idea of the research and supervised the process. The first draft was written by EEGM, and all authors commented on previous versions of the manuscript. All authors read and approved the final manuscript.

Declaration of Competing Interest

The authors declare that the research was conducted in the absence of any commercial or financial relationships that could be construed as potential conflict of interest.

Data Availability

All data generated during the research are available at the following link:

https://drive.google.com/drive/folders/1-l_Ae4IBNzQBB17RVepfYN3TeHNyfaKv?usp=sharing

Acknowledgment

This work was supported by Agencia Estatal de Investigación (PID2019-106231RB-I00), Institute Smart Cities and Public University of Navarra PhD Student grants. SM-E would like to express her gratitude for the Fellowship supported by the Royal Academy of Engineering under the Leverhulme Trust Research Fellowships scheme (LTRF2021\17130).

References

[1] Del Villar, I., Zamarreño, C. R., Hernaez, M., Arregui, F. J., & Matias, I. R. (2009). Lossy mode resonance generation with indium-tin-oxide-coated optical fibers for sensing applications. Journal of Lightwave Technology, 28(1), 111-117. https://doi.org/10.1109/JLT.2009.2036580

[2] Del Villar, I., Hernaez, M., Zamarreño, C. R., Sánchez, P., Fernández-Valdivielso, C., Arregui, F. J., & Matias, I. R. (2012). Design rules for lossy mode resonance based sensors. Applied optics, 51(19), 4298-4307. https://doi.org/10.1364/AO.51.004298

[3] Del Villar, I., Arregui, F. J., Zamarreño, C. R., Corres, J. M., Bariain, C., Goicoechea, J., ... & Matias, I. R. (2017). Optical sensors based on lossy-mode resonances. Sensors and Actuators B: Chemical, 240, 174-185. https://doi.org/10.1016/j.snb.2016.08.126

[4] Zamarreño, C. R., Sanchez, P., Hernaez, M., Del Villar, I., Fernandez-Valdivielso, C., Matias, I. R., & Arregui, F. J. (2010, October). LMR-based optical fiber refractometers based on transparent conducting and semiconducting oxide coatings: A comparative study. In 2nd Workshop on Specialty Optical Fibers and Their Applications (WSOF-2) (Vol. 7839, pp. 193-196). SPIE. https://doi.org/10.1117/12.867063

[5] Del Villar, I., Bohorquez, D. L., Caputo, D., Buzzin, A., Chiavaioli, F., Baldini, F., ... & Matias, I. R. (2020, October). Lossy mode resonance sensors based on tungsten oxide thin films. In 2020 IEEE SENSORS (pp. 1-4). IEEE. https://doi.org/10.1109/SENSORS47125.2020.9278899

[6] Ozcariz, A., Zamarreño, C. R., Zubiate, P., & Arregui, F. J. (2017). Is there a frontier in sensitivity with Lossy mode resonance (LMR) based refractometers?. Scientific reports, 7(1), 10280. https://doi.org/10.1038/s41598-017-11145-9

[7] Usha, S. P., & Gupta, B. D. (2017). Performance analysis of zinc oxide-implemented lossy mode resonance-based optical fiber refractive index sensor utilizing thin film/nanostructure. Applied optics, 56(20), 5716-5725. https://doi.org/10.1364/AO.56.005716

[8] Paliwal, N., & John, J. (2014, October). Sensitivity enhancement of aluminium doped zinc oxide (AZO) coated lossy mode resonance (LMR) fiber optic sensors using additional layer of oxides. In Laser Science (pp. JTu3A-40). Optica Publishing Group. https://doi.org/10.1364/FIO.2014.JTu3A.40

[9] Ozcariz, A., Martinez, I., Zamarreño, C. R., & Arregui, F. J. (2018, November). Development of copper oxide thin film for lossy mode resonance-based optical fiber sensor. In Proceedings (Vol. 2, No. 13, p. 893). MDPI. https://doi.org/10.3390/proceedings2130893

[10] Sharma, S., & Gupta, B. D. (2018). Lossy Mode Resonance-Based Fiber Optic Sensor for the Detection of As (III) Using $\alpha $-Fe 2 O 3/SnO 2 Core–Shell Nanostructures. IEEE Sensors Journal, 18(17), 7077-7084. https://doi.org/10.1109/JSEN.2018.2851610

[11] Zamarreño, C. R., Hernáez, M., Del Villar, I., Matías, I. R., & Arregui, F. J. (2011). Optical fiber pH sensor based on lossy-mode resonances by means of thin polymeric coatings. Sensors and Actuators B: Chemical, 155(1), 290-297. https://doi.org/10.1016/j.snb.2010.12.037

[12] Fuentes, O., Corres, J. M., Matias, I. R., & Del Villar, I. (2019). Generation of lossy mode resonances in planar waveguides toward development of humidity sensors. Journal of Lightwave Technology, 37(10), 2300-2306. https://doi.org/10.1109/JLT.2019.2902045

[13] Matias, I. R., Del Villar, I., & Corres, J. M. (2023). Lossy mode resonance based sensors in planar configuration: a review. IEEE Sensors Journal. https://doi.org/10.1109/JSEN.2023.3243937

[14] Tiwari, D., Mullaney, K., Korposh, S., James, S. W., Lee, S. W., & Tatam, R. P. (2017). An ammonia sensor based on Lossy Mode Resonances on a tapered optical fibre coated with porphyrin-incorporated titanium dioxide. Sensors and Actuators B: Chemical, 242, 645-652. https://doi.org/10.1016/j.snb.2016.11.092

[15] Zamarreño, C. R., Hernaez, M., Del Villar, I., Matias, I. R., & Arregui, F. J. (2010). Tunable humidity sensor based on ITO-coated optical fiber. Sensors and Actuators B: Chemical, 146(1), 414-417. https://doi.org/10.1016/j.snb.2010.02.029

[16] Zamarreño, C. R., Hernaez, M., Sanchez, P., Del Villar, I., Matias, I. R., & Arregui, F. J. (2011). Optical fiber humidity sensor based on lossy mode resonances supported by TiO2/PSS coatings. Procedia Engineering, 25, 1385-1388. https://doi.org/10.1016/j.proeng.2011.12.342

[17] Sanchez, P., Zamarreño, C. R., Hernaez, M., del Villar, I., Matias, I. R., & Arregui, F. J. (2013, May). Humidity sensor fabricated by deposition of SnO2 layers onto optical fibers. In Fifth European Workshop on Optical Fibre Sensors (Vol. 8794, pp. 46-49). SPIE. https://doi.org/10.1117/12.2026091

[18] Zamarreño, C. R., Hernaez, M., Del Villar, I., Matias, I. R., & Arregui, F. J. (2011, October). Lossy mode resonance-based optical fiber humidity sensor. In SENSORS, 2011 IEEE (pp. 234-237). IEEE. https://doi.org/10.1109/ICSENS.2011.6127124

[19] Rivero, P. J., Urrutia, A., Goicoechea, J., & Arregui, F. J. (2012). Optical fiber humidity sensors based on Localized Surface Plasmon Resonance (LSPR) and Lossy-mode resonance (LMR) in overlays loaded with silver nanoparticles. Sensors and Actuators B: Chemical, 173, 244-249. https://doi.org/10.1016/j.snb.2012.07.010

[20] Sanchez, P., Zamarreño, C. R., Hernaez, M., Del Villar, I., Fernandez-Valdivielso, C., Matias, I. R., & Arregui, F. J. (2011). Lossy mode resonances toward the fabrication of optical fiber humidity sensors. Measurement Science and Technology, 23(1), 014002. https://doi.org/10.1088/0957-0233/23/1/014002

[21] Ascorbe, J., Corres, J. M., Matias, I. R., & Arregui, F. J. (2016). High sensitivity humidity sensor based on cladding-etched optical fiber and lossy mode resonances. Sensors and Actuators B: Chemical, 233, 7-16. https://doi.org/10.1016/j.snb.2016.04.045

[22] Urrutia, A., Goicoechea, J., Rivero, P. J., Pildain, A., & Arregui, F. J. (2018). Optical fiber sensors based on gold nanorods embedded in polymeric thin films. Sensors and Actuators B: Chemical, 255, 2105-2112. https://doi.org/10.1016/j.snb.2017.09.006

[23] Bohorquez, D. L., Del Villar, I., Corres, J. M., & Matias, I. R. (2020). Generation of lossy mode resonances in a broadband range with multilayer coated coverslips optimized for humidity sensing. Sensors and Actuators B: Chemical, 325, 128795. https://doi.org/10.1016/j.snb.2020.128795

[24] Hernaez, M., Mayes, A. G., & Melendi-Espina, S. (2017). Graphene oxide in lossy mode resonance-based optical fiber sensors for ethanol detection. Sensors, 18(1), 58. https://doi.org/10.3390/s18010058

[25] Usha, S. P., Mishra, S. K., & Gupta, B. D. (2015). Fiber optic hydrogen sulfide gas sensors utilizing ZnO thin film/ZnO nanoparticles: A comparison of surface plasmon resonance and lossy mode resonance. Sensors and Actuators B: Chemical, 218, 196-204. https://doi.org/10.1016/j.snb.2015.04.108

[26] Vitoria, I., Gallego, E. E., Melendi-Espina, S., Hernaez, M., Ruiz Zamarreño, C., & Matías, I. R. (2023). Gas Sensor Based on Lossy Mode Resonances by Means of Thin Graphene Oxide Films Fabricated onto Planar Coverslips. Sensors, 23(3), 1459. https://doi.org/10.3390/s23031459

[27] Lerf, A., He, H., Forster, M., & Klinowski, J. (1998). Structure of graphite oxide revisited. The Journal of Physical Chemistry B, 102(23), 4477-4482. https://doi.org/10.1021/jp9731821

[28] He, H., Klinowski, J., Forster, M., & Lerf, A. (1998). A new structural model for graphite oxide. Chemical physics letters, 287(1-2), 53-56. https://doi.org/10.1016/S0009-2614(98)00144-4

[29] Goya, K., Mori, A., Tokita, S., Yasuhara, R., Kishi, T., Nishijima, Y., ... & Uehara, H. (2021). Broadband mid-infrared amplified spontaneous emission from Er/Dy co-doped fluoride fiber with a simple diode-pumped configuration. Scientific Reports, 11(1), 5432. https://doi.org/10.1038/s41598-021-84950-y

[30] Popa, D., & Udrea, F. (2019). Towards integrated mid-infrared gas sensors. Sensors, 19(9), 2076. https://doi.org/10.3390/s19092076

[31] Hahn, H. D., Dämbkes, G., Rupprich, N., Bahl, H., & Frey, G. D. (2000). Butanols. Ullmann's Encyclopedia of Industrial Chemistry. https://doi.org/10.1002/14356007.a04_463.pub3

[32] Song, G., Qin, T., Liu, H., Xu, G. B., Pan, Y. Y., Xiong, F. X., ... & Chen, Z. D. (2010). Quantitative breath analysis of volatile organic compounds of lung cancer patients. Lung cancer, 67(2), 227-231. https://doi.org/10.1016/j.lungcan.2009.03.029

[33] ICSC. International Chemical Safety Cards leaflet. (April, 2005). https://www.ilo.org/dyn/icsc/showcard.display?p_lang=es&p_card_id=0111&p_version=2. (Accessed 2 Feb 3023).

[34] McLain, V. C. (2008). Final report of the addendum to the safety assessment of n-butyl alcohol as used in cosmetics. International Journal of Toxicology, 27, 53-69. https://doi.org/10.1080/10915810802244504

[35] Zhao, Z., Jiang, D., Xue, Y., Sun, Y., Zhang, W., Li, P., ... & Hu, J. (2021). Synthesis and characterization of AuNPs-modificated Fe2O3/ZnFe2O4 heterostructures for highly sensitive 1-butanol detection. Journal of Materials Science, 56(30), 16963-16975. https://doi.org/10.1007/s10853-021-06380-5

[36] Bhat, P., & Nagaraju, P. (2019). Synthesis and characterization of ZnO-MWCNT nanocomposites for 1-butanol sensing application at room temperature. Physica B: Condensed Matter, 570, 139-147. https://doi.org/10.1016/j.physb.2019.06.008

[37] Fan, X., & Du, B. (2011). Selective detection of trace 1-butanol by QCM sensor coated with copolymer P (HEMA-co-MA). Sensors and Actuators B: Chemical, 160(1), 724-729. https://doi.org/10.1016/j.snb.2011.08.055

[38] Bhat, P., & Kumar, S. N. (2022, March). Real-time detection of 1-butanol VOCin an indigenously developed Gas chamber. In IOP Conference Series: Materials Science and Engineering (Vol. 1221, No. 1, p. 012005). IOP Publishing. https://doi.org/10.1088/1757-899X/1221/1/012005

[39] Men, D., Feng, S., Liu, G., Hang, L., & Zhang, T. (2020). A Sensitive “Optical Nose” for Detection of Volatile Organic Molecules Based on Au@ MOFs Nanoparticle Arrays through Surface-Enhanced Raman Scattering. Particle & Particle Systems Characterization, 37(4), 1900452. https://doi.org/10.1002/ppsc.201900452

[40] Zhao, W. M., & Wang, Q. (2022). Analytical Solutions to Fundamental Questions for Lossy Mode Resonance. Laser & Photonics Reviews, 2200554. https://doi.org/10.1002/lpor.202200554

[41] 2012 Crystran Ltd., (2012) Calcium Fluoride Optical Properties Calcium Fluoride Optical Material. CRYSTRAN UV - VISIBLE - IR SPECIALIST OPTICS. https://www.crystran.co.uk/optical-materials/calcium-fluoride-caf2. (Accessed 2 Feb 2023)

[42] Hoffman, D., Singh, B., & Thomas III, J. H. (1997). Handbook of vacuum science and technology. Elsevier.

[43] Hernaez, M., Acevedo, B., Mayes, A. G., & Melendi-Espina, S. (2019). High-performance optical fiber humidity sensor based on lossy mode resonance using a nanostructured polyethylenimine and graphene oxide coating. Sensors and Actuators B: Chemical, 286, 408-414. https://doi.org/10.1016/j.snb.2019.01.145

[44] Liu, R., Gong, T., Zhang, K., & Lee, C. (2017). Graphene oxide papers with high water adsorption capacity for air dehumidification. Scientific Reports, 7(1), 9761. https://doi.org/10.1038/s41598-017-09777-y

[45] Medhekar, N. V., Ramasubramaniam, A., Ruoff, R. S., & Shenoy, V. B. (2010). Hydrogen bond networks in graphene oxide composite paper: structure and mechanical properties. ACS nano, 4(4), 2300-2306. https://doi.org/10.1021/nn901934u

[46] Ozcariz, A., Piña-Azamar, D. A., Zamarreño, C. R., Dominguez, R., & Arregui, F. J. (2019). Aluminum doped zinc oxide (AZO) coated optical fiber LMR refractometers—An experimental demonstration. Sensors and Actuators B: Chemical, 281, 698-704. https://doi.org/10.1016/j.snb.2018.10.158

[47] Canosa, J., Rodriguez, A., & Tojo, J. (1998). Dynamic viscosities of (methyl acetate or methanol) with (ethanol, 1-propanol, 2-propanol, 1-butanol, and 2-butanol) at 298.15 K. Journal of Chemical & Engineering Data, 43(3), 417-421. https://doi.org/10.1021/je9702302

[48] Viscosidad dinámica (tenacidad y coeficiente de fricción interna). https://www.flottweg.com/es/wiki/tecnica-de-separacion/viscosidad-dinamica/ Accessed (2 Feb 2023)